




Performance Analysis of MIMO SWIPT Relay Network with Imperfect CSI

Tran Manh Hoang¹ · Xuan Nam Tran¹ · Nguyen Thanh¹ · Le The Dung² 

Published online: 5 November 2018
© Springer Science+Business Media, LLC, part of Springer Nature 2018

Abstract

In this paper, we consider a dual-hop multiple-input multiple-output (MIMO) simultaneous wireless information and power transfer (SWIPT) relay network, where the source node (SN) uses a transmission antenna selection (TAS) scheme to concurrently send information and energy to the single-antenna relay node (RN). This helps to utilize the harvested energy to forward the received signal. In addition, the destination node (DN) employs the maximum ratio combining (MRC) scheme to process this forwarded signal. The performance of this MIMO SWIPT relay system is investigated in imperfect channel state information (CSI) condition. Specifically, we derive the exact and approximate closed-form expressions for the outage probability, the average capacity, and the symbol error probability (SEP). This is the first time the exact and approximate formulas for the SEP of the energy harvesting networks are investigated. The Monte Carlo simulation results are provided to demonstrate the relevance of the developed analytical results, showing that the system's performance is significantly impacted by the CSI imperfection, the number of antennas, and the energy harvesting duration.

Keywords MIMO · Relay · Transmit antenna selection · Maximum ratio combining · Energy harvesting · Imperfect CSI

Nomenclature

$Pr(\cdot)$ Probability function
 $f_U(u)$ Probability density function (PDF)
 $F_U(u)$ Cumulative distribution function (CDF)
 $\Gamma(\cdot)$, Gamma function
 $\Gamma(\cdot, \cdot)$ Incomplete gamma function
 $\mathcal{CN}(\mu, \sigma^2)$ Circularly symmetric complex normal distribution with mean μ and variance σ^2
 $\mathbb{E}\{\cdot\}$ Statistical expectation operator

$\mathcal{K}_n(\cdot)$ Modified Bessel function of the second kind of order n
 $E_n(\cdot)$ Integral exponential function of order n
 $W_{\ell, \mu}(\cdot)$ Whittaker function [32]

1 Introduction

The energy supply for electronic devices has become a hot studying topic in fifth generation (5G) and sixth generation (6G) network.¹ To enhance the energy efficiency in 5G wireless networks, the authors of [2] proposed novel resource allocation schemes for the energy efficiency maximization problem in emerging scenarios of wireless networks, including small cell, massive MIMO, massive MIMO HetNets and cell-free. Additionally, there is another way to address the energy issues, i.e. to harvest energy from ambient energy sources.

The energy harvesting (EH) from ambient energy sources has become a promising solution for energy-constrained electronic devices, which are supported by limited energy sources such as batteries. In some special applications, charging battery is too expensive or even impossible, e.g. sensor network working under toxic environment or body

✉ Le The Dung
dung.t.le@ieee.org

Tran Manh Hoang
tranmanhhoang@tcu.edu.vn

Xuan Nam Tran
namtx@mta.edu.vn

Nguyen Thanh
ngthanh1702@gmail.com

¹ Faculty of Radio Electronics, Le Quy Don Technical University, Hanoi, Vietnam

² Department of Radio and Communication Engineering, Chungbuk National University, Cheongju, Korea

¹6G will start entering the market by 2026 [1]

area network, etc. In addition to some natural energy sources such as solar, wind, etc., radio frequency (RF) signal can be also utilized as an effective source for energy harvesting. Compared with other kinds of sources, RF-based energy harvesting, also called wireless energy transfer, has some unique advantages. Since it is an active energy supplying method, RF energy harvesting can provide more reliable energy flow to guarantee the system performance.

Nowadays, Internet of Things (IoT) has received increasing attentions from both industry and academia. It is also considered as an important means of wireless connections for the fourth industrial revolution. IoT was included in the advanced wireless standards such as the fourth generation (4G) and is currently being considered for the fifth generation (5G) of mobile communications. RF energy transfer and harvesting techniques have recently become alternative methods to power the next generation wireless networks. Specially for 5G network, as this emerging technology enables proactive energy replenishment of wireless devices, it is advantageous in supporting applications with quality of service (QoS) requirements.

The key idea of EH-RF, firstly proposed in [3], is to encourage nodes to harvest energy from their received RF information-bearing signals. However, it is not practical for a receiver architecture to decode signals and to harvest energy at the same time due to practical limitations [4]. The conventional receiver architecture for information receiving is not operationally optimal for energy harvesting. The reason is that the information receiver and energy harvester operate at different signal threshold sensitivities (e.g., -10 dBm for energy harvester, and -60 dBm for information receiver) [5]. Motivated by this issue, Zhou et al introduced two practical receiver architectures [6], namely, the power splitting (PS) and the time switching (TS) architectures. These schemes were also proposed for cooperative networks, which considered both amplify-and-forward (AF) and decode-and-forward (DF) protocols [7, 8]. A more general SWIPT cooperative relaying network, i.e., multiuser multirelay cooperative network, was considered in [9]. In this work, the outage performances of DF, variable-gain AF, and fixed-gain AF strategies were investigated. Moreover, two new relay-destination selection schemes, namely the direct links plus opportunistic CSI-based selection scheme and the direct links plus partial CSI-based selection scheme, were also proposed to drastically reduce the numbers of CSI estimations and comparisons of potential links compared with the optimal joint relay-destination selection scheme. Regarding to the efficiency aspect of the energy harvester, Dong et al investigated a more effective architecture [10], that is not a traditional linear energy harvesting process. Instead, the output power is non-linearly related to the input power at the relay node with an AF protocol.

A potential emerging technique for 5G networks is the non-orthogonal multiple access (NOMA). The authors in [11–14] investigated the SWIPT schemes to prolong the lifetime of devices in NOMA networks. In these works, the outage probabilities are analyzed. In addition, a generalized SWIPT architecture, i.e. the hybrid time-switching/power-splitting (TS/PS) EH receiver was considered in [11]. However, since the TS/PS and successive interference cancellation architectures must be designed at near users, this SWIPT model increases the complexity of the near users.

To the best of our knowledge, relay networks with energy harvesting policy are currently considered with the general system configuration of three nodes in cooperation. However, there is lack of discussions on the topic of analyzing the system error probability. Moreover, most of the aforementioned works on EH-MIMO systems assumed the perfect channel state information (CSI) [15–18], also only analyzed the EH-MIMO point-to-point system [19–22] but not the EH-MIMO relaying networks. On the other hand, the imperfect CSI was only taken into consideration in cognitive underlay multihop networks [23], in secrecy cooperative networks [24] and in MIMO network with transmit antenna selection to enhance secure information [25].

The MIMO systems are considered as a promising technique and found its way in several recent wireless communication networks, aiming at further improving the system Quality of Service (QoS). Therefore, it is meaningful to investigate and analyze the performance of MIMO system taking into account the impact of some practical issues. The combination of MIMO technique and energy harvesting is thus an interesting topic. Applications of this configuration are broad, for example, in a sensor network, healthcare, medicine, environment managing, military operations, etc. In practice, due to the complex time-varying wireless communication environment that impacts to the channel gains, their severe amplitude and phase fluctuations could significantly degrade the system performance. When having error in estimating amplitude of the channel gain, automatic gain control (AGC) can be used to somehow properly scale the received signal. However, even if in the absence of noise, when the phase component is estimated in error, it will be very difficult to (phase) compensate for the received signal. Hence, in this work, we study the impacts of the CSI imperfection on the MIMO relaying network with energy harvesting and analyze the system performance. Then, this approach could have both theoretical and practical meanings.

There are several works investigating the energy harvesting under imperfect CSI. In [26], Lee and Hong proposed an energy-efficient power reallocation scheme using iterative method. Benkhelifa et al investigated a MIMO DF

two-hop system where the relay node harvests the self-energy recycle and CSI is entirely unknown in all nodes [27]. The main contribution of this work is to maximize the achievable transmission rate of the overall system by optimizing the source/relay pre-coders. The performance of the cognitive relay network with imperfect CSI and energy harvesting is studied in [28]. In other work, Zhang and Pan investigated the impact of the outdated CSI for the wireless powered dual-hop relaying MIMO system with non-linear energy harvesting at relay node [29]. However, since only focusing on the capacity or outage performance, the above mentioned works leaved out an importance criterion, namely the system error probability performance. Specially, the standard performance characteristics of diversity systems operating in fading channels were not evaluated and so on the effects of energy harvesting duration on the system performance.

Motivated by these issues, this paper proposes and investigates a MIMO system with RF energy harvesting to improve energy efficiency. Here, the transmit antenna selection (TAS) and maximum ratio combining (MRC) are employed at the source and destination nodes, respectively. The system performance is investigated in terms of the outage probability, ergodic capacity, and symbol error probability (SER) under imperfect CSI condition. Based on these outputs and result in [30] we conclude that when using 0.33 time block for energy harvesting, the maximum loss in signal-to-noise ratio (SNR) of this system is about 1.7 dB compared to the scheme without EH at relay node (at $SER = 5.10^{-6}$). The contributions of the paper are summarized as follow:

- We propose a MIMO relaying system with the relay node having limited energy and being able to transfer power to recharge its batteries. We then consider the impact of CSI imperfection on the performance of TAS. When employing multiple antennas at the source and the destination nodes, the system performance is improved at the cost of increasing the complexity. Fortunately, the antennas configurations and RF chains are easily implemented by the current modern technologies. Configuring multiple antennas at the relay node will increase its complexity because the harvester is also deployed here [31]. For this reason, the advantage of our proposed model is to minimize the hardware and computation complexity of the relay node. Thus, this configuration prolongs the lifetime of the network with relay nodes being independent to or, at least, using reduced power supply compared to other present schemes.
- We derive the closed-form outage probability, ergodic capacity and average symbol error probability. Due to the relative challenge in deriving the cumulative

distribution functions (CDFs) of SNR in MIMO-SWIPT system with imperfect CSI, the symbol error probability expressions has not been analyzed before. Recall that, the advantages of the MIMO system are exploited: SEP performance improvement in the data transmission phase and power efficiency enhancement in the energy harvesting phase. This comes at the price of increasing system complexity (mainly at the source and destination nodes) and could be afforded by the current technology advancements.

- The accurateness of our analysis is validated by simulations. Besides, the numerical results indicate that the diversity order of this MIMO-SWIPT system is equivalent to the number of antennas configured at the destination node. In this paper, we provide both the analysis and the simulation results, which are more advantageous than previous works in the literature where only simulation results were presented.

The rest of this paper is organized as follows. Section 2 describes the system model, its operation and characterizes the channel. The performance features are then analyzed in Section 3. Section 4 presents and discusses numerical results. Finally, conclusions are drawn in Section 5.

2 System model

We consider a MIMO dual-hop relay system where the energy-limited relay node (R) assists the source node (S) in communicating with the destination node (D) as illustrated in Fig. 1. In this system, S and D are equipped with N_S and N_D antennas, respectively, while R has one (transmit/receive) antenna and the system operates in half-duplex mode. S and D have fixed power supplies but R is powered by wireless power transferred from S. Assume that R has separate EH receiver and RF transceiver, hence, it can harvest energy and communicate data independently. The RF EH is in-band, namely, R can harvest RF energy from the same frequency band as that of data communication. Further, suppose that R employs Decode-and-Forward (DF) protocol.

The direct link from S to D is assumed not available due to far distance or shadowing fading. All fading channels

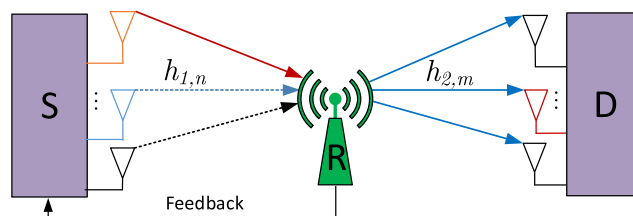


Fig. 1 The proposed MIMO SWIPT relay network

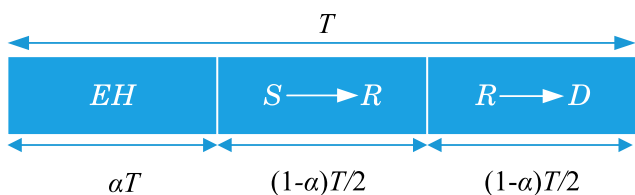


Fig. 2 Time switching-based relaying (TSR) protocol

are quasi-static independent and identically distributed (i.i.d), i.e. the fading coefficients remain fixed during the transmission of one symbol block but vary independently from block to block.

Denote $h_{1,n} \sim \mathcal{CN}(\mu, \Omega_{1,n}), n = 1, 2, \dots, N_S$ and $h_{2,m} \sim \mathcal{CN}(\mu, \Omega_{2,m}), m = 1, 2, \dots, N_D$ respectively as the channel coefficients from the S's n th antenna to the R's (receive) antenna and from the R's (transmit) antenna to the D's m th antenna, where $\Omega_{1,n} = \mathbb{E}\{|h_{1,n}|^2\}$ and $\Omega_{2,m} = \mathbb{E}\{|h_{2,m}|^2\}$. In this model, we assume that spaces between antennas are large enough so that these antennas are uncorrelated and that all channels from the S's n th antenna to the R's antenna have the same average channel gains, and so on for ones from R's antenna to the D's m th antenna, i.e., $\Omega_{1,n} = \Omega_1$ and $\Omega_{2,m} = \Omega_2$. Further, without loss of generality, we assume that all device-to-device links are Rayleigh-distributed. Hence, the channel gains $|h_{1,n}|^2$ and $|h_{2,m}|^2$ are exponential random variables (RVs).

The time switching (TS) architecture [8] with illustration in Fig. 2, is supposed for the operation of the relay node.² In this figure, T is one block time in which a certain block of information is transmitted from the source node to the destination node. The communication process is split into three time slots, where the first slot, αT (with $0 \leq \alpha \leq 1$) is used for energy harvesting at R. The remaining block time, $(1 - \alpha)T$, divided into two equal slots, is used for information transmission. The first half of that, $(1 - \alpha)T/2$, is used for the S-to-R information transmission and the remaining half, $(1 - \alpha)T/2$, is used for the R-to-D information transmission. In the case where R does not have an energy buffer to store the harvested energy, the harvest-use (HU) architecture [33] can be used.

For the operation of TAS in S, the following procedure is carried out: S regularly supervises the channel quality by transmitting a set of pilot sequences from each antenna one by one, R compares the received signals of all antennas, and sends feedback to S about the selected antenna index corresponding to the signal with maximum magnitude. Then, S selects the single antenna out of set N_S that provides the highest instantaneous channel gain, to transmit data to

R. Thus, the channel gain of TAS is modeled as $|\hat{h}_{SR}|^2 = \max_{n \in 1 \dots N_S} |\hat{h}_{1,n}|^2$.

Aiming at mitigating the adverse effects of fading, TAS schemes are usually accompanied with maximal-ratio combining (MRC) technique at D. As widely known, MRC technique represents a trade-off between performance and complexity. On the one hand, MRC is the optimal linear combining technique yielding the best performance, but on the other hand, its implementation is more complex because it requires multiple channel estimations and also multiple RF chains, each for one antenna. However, to improve system performance the MRC technique is applied here.

The main objective of this paper is to focus on investigating impact of CSI imperfection on the MIMO relay system where the RF energy harvesting is applied. Due to the time-varying characteristics of the channel, the S-to-D channel might alter whenever the feedback delay is larger than the transmission block length T as depicted in Fig. 2. Simply, we assume that the correlation coefficients, $\rho_{1,n}$, between the current channel coefficient $\hat{h}_{1,n}$ and the past channel coefficient $h_{1,n}$ are the same, i.e., $\rho_{1,n} = \rho, n = 1, 2, \dots, N_S$.

Using the Markov chain model for the channel state evolution, \hat{h}_{SR} is related to h_{SR} by the following relationship [34]

$$\hat{h}_{SR} = \rho h_{SR} + \sqrt{1 - \rho^2} \varepsilon_{SR}, \tag{1}$$

where $0 \leq \rho \leq 1$. This coefficient³ can be viewed as a measure of the channel fluctuation rate and is related solely to the time delay. ε_{SR} is an error term due to temporal changes in the channel, which is modeled by a circular symmetric complex Gaussian random variable. As elaborately discussed in [36], all random variables $\{\hat{h}_{SR}, h_{SR}, \varepsilon_{SR}\}$ are modeled as $\mathcal{CN}(\mu, \sigma^2)$. For a slowly varying channel, the average fading power is supposed to remain constant over the time delay, i.e., $\mathbb{E}\{|\hat{h}_{1,i}|^2\} = \mathbb{E}\{|h_{1,i}|^2\}$.

We assume that the energy is only harvested from the received signal during αT in each period.⁴ Hence, the harvested energy is given by [8, eq.(2)].

$$E_h = \alpha T \eta P_S \max_{n=1, \dots, N_S} |\hat{h}_{1,n}|^2, \tag{2}$$

where η is the energy conversion efficiency whose values depend on the quality of the harvester, $0 < \eta < 1$, and P_S is the S's transmit power.

According to HU architecture, R uses all harvested energy yielded in the harvesting phase to forward the

²The proposed analysis approach can also be applied to the power spitting EH model [6].

³The covariance between x and y is given as [35] $\rho = \frac{cov(x,y)}{var(x)var(y)}$.

⁴Recently, there are several articles investigating EH from the co-channel interference deployed in the future 5G network, and EH from the interference in IoT network.

received data to D. Hence, the transmit power of R is given by

$$P_R = \frac{2\alpha\eta P_S}{(1-\alpha)} \max_{n=1, \dots, N_S} |\hat{h}_{1,n}|^2 = \phi P_S \max_{n=1, \dots, N_S} |\hat{h}_{1,n}|^2, \quad (3)$$

where $\phi = 2\alpha\eta/(1-\alpha)$.

The remaining communication takes place in two equal time slots. In the first time slot, S transmits signal to R through the selected antenna. Whereby, the received signal at R, y_R is given by

$$y_R = \sqrt{P_S} \hat{h}_{SR} x_S + n_R, \quad (4)$$

where $n_R \sim \mathcal{CN}(0, \sigma_R^2)$ is the additive white Gaussian noise (AWGN) at the relay, and x_S is the S's modulated signal.

In the second time slot, R uses the harvested energy to forward the received signal to D after re-encode.⁵ The received signals are then combined at D using MRC. Hence, the baseband signal at D is given as

$$y_D = \sqrt{P_R} \sum_{m=1}^{N_D} h_{2,m} \tilde{x}_S + n_D, \quad (5)$$

where \tilde{x}_S is the re-encode symbols at D and $n_D \sim \mathcal{CN}(0, \sigma_D^2)$ is the AWGN at D.

3 Performance analysis

3.1 Statistics of the end-to-end SNR

To evaluate the system performance, it is required the cumulative distribution functions (CDF) and the probability density function (PDF) of the end-to-end SNR.

Firstly, we derive the CDF and PDF of the output instantaneous SNR of the link from the best antenna chosen at S to the antenna at R under the impact of the imperfect CSI. As described in [35], the channel gain of the first hop, $|h_{1,i}|^2$, is considered as having exponential distribution. Hence, the PDF and CDF are correspondingly given by Eqs. 6 and 7, i.e.,

$$f_{|h_{1,i}|^2}(y) = \frac{1}{\Omega_1} \exp\left(-\frac{y}{\Omega_1}\right), \quad (6)$$

and

$$F_{|h_{1,i}|^2}(y) = 1 - \exp\left(-\frac{y}{\Omega_1}\right). \quad (7)$$

Let $h_{1,(1)} \leq h_{1,(2)} \leq \dots \leq h_{1,(N_S)}$ be the order statistics obtained by arranging $\{h_{1,n}\}_{n=1}^{N_S}$ in an increasing order of magnitude. When the n th antenna is selected to transmit the

modulated signal, the corresponding highest instantaneous channel gain, $h_{1,n}$, has the PDF expressed as [35, 7-14].⁶

$$f_{|h_{1,n}|^2}(y) = N_S \left[F_{|h_{1,i}|^2}(y) \right]^{N_S-1} f_{|h_{1,i}|^2}(y) = \sum_{n=1}^{N_S} \binom{N_S}{n} (-1)^{n-1} \frac{n}{\Omega_1} \exp\left(-\frac{ny}{\Omega_1}\right). \quad (8)$$

The relationship between the fading channel amplitudes $\hat{h}_{1,n}$ and $h_{1,n}$ is described by the marginal distribution, $f_{|\hat{h}_{1,n}|^2}(x) = \int_0^\infty f_{|\hat{h}_{1,n}|^2, |h_{1,n}|^2}(x, y) dy$ or can be recast, according to the conditional probability, as

$$f_{|\hat{h}_{1,n}|^2}(x) = \int_0^\infty f_{|\hat{h}_{1,n}|^2, |h_{1,n}|^2}(x|y) f_{|h_{1,n}|^2} dy, \quad (9)$$

where

$$f_{|\hat{h}_{1,n}|^2, |h_{1,n}|^2}(x|y) = \frac{f_{|\hat{h}_{1,i}|^2, |h_{1,i}|^2}(x, y)}{f_{|h_{1,i}|^2}(y)}. \quad (10)$$

Based on the joint PDF of two correlated fading channel amplitudes, defined in [37, eq. 9.389], we can recast into the form of Rayleigh fading channel as

$$f_{|\hat{h}_{1,i}|^2, |h_{1,i}|^2}(x, y) = \frac{1}{(1-\rho^2)\Omega_1^2} e^{-\frac{x+y}{(1-\rho^2)\Omega_1}} I_0\left(\frac{2\rho\sqrt{xy}}{(1-\rho^2)\Omega_1}\right), \quad (11)$$

where $I_0(x)$ is modified Bessel function of first kind of zero-th order, parameter ρ can be viewed as a measure of the channel estimation quality.

Substitute (6) and (11)–(10), then replace (8) and (10)–into (9), after that use [32, 6.614.3], this leads to the form of $\int_0^\infty e^{-\alpha z} I_0(2\sqrt{\beta z}) dz = (1/\alpha) \exp(\beta/\alpha)$. Hence, after performing some manipulations and simplifications, we have the PDF of SNR on the first hop as

$$f_{|\hat{h}_{1,n}|^2}(x) = \sum_{n=1}^{N_S} \binom{N_S}{n} \frac{(-1)^{n-1} n}{\Omega_1(1+(n-1)(1-\rho^2))} \times \exp\left(-\frac{nx}{\Omega_1(1+(n-1)(1-\rho^2))}\right). \quad (12)$$

Now, consider the operation of N_D branch using MRC.⁷ Assume that each branch are independent and identically distributed (iid), and are Rayleigh distributed. The output SNR accords to a sum of independent exponential random

⁵We assume that all energy harvested from the RF signals is consumed by the relay for forwarding the information to the destination.

⁶To obtain (8), we use the probability that any k of the N elements are below y . Hence, we need to enumerate the number of combinations of k out of N variables. This is merely the binomial coefficient. Then, we differentiate the result with respect to y .

⁷We consider the MRC scheme employed at D since MRC always outperforms any other diversity combining schemes.

variables [38]. Under the assumption of perfect channel estimation at D, the PDF of the combined output SNR from N_D diversity branches follows the χ^2 distribution with $2N_D$ degrees of freedom [39].

$$f_{\gamma_{MRC}}(\gamma) = \frac{\gamma^{N_D-1}}{\Gamma(N_D)\Omega_2^{N_D}} \exp\left(-\frac{\gamma}{\Omega_2}\right), \tag{13}$$

where $\Gamma(\cdot)$ is Gamma function.

From the PDF in Eq. 13, we have CDF of γ_{MRC} in the form of

$$F_{\gamma_{MRC}}(\gamma) = \frac{1}{\Gamma(N_D)\Omega_2^{N_D}} \int_0^\gamma \gamma'^{N_D-1} \exp\left(-\frac{\gamma'}{\Omega_2}\right) d\gamma'. \tag{14}$$

Applying [32, 3.381.1], then $F_{\gamma_{MRC}}(\gamma)$ is recast as

$$\begin{aligned} F_{\gamma_{MRC}}(x) &= \frac{1}{\Gamma(N_D)} \gamma\left(N_D, \frac{x}{\Omega_2}\right) \\ &= 1 - \frac{1}{\Gamma(N_D)} \Gamma\left(N_D, \frac{x}{\Omega_2}\right), \end{aligned} \tag{15}$$

where $\Gamma(\cdot, \cdot)$ denotes the lower incomplete Gamma function.

Based on the CDF and PDF of each hop, the CDF of end-to-end SNR is derived as follows. From the Eqs. 4 and 5 the instantaneous SNRs of the S-to-R and R-to-D links are correspondingly given as

$$\gamma_{SR} = \frac{P_S}{\sigma_R^2} \max_{n=1, \dots, N_S} |\hat{h}_{1,n}|^2, \tag{16}$$

$$\gamma_{RD} = \frac{P_R}{\sigma_D^2} \sum_{m=1}^{N_D} |h_{2,m}|^2. \tag{17}$$

From Eqs. 17 and 3 the SNR of the R-to-D link, γ_{RD} is computed as

$$\gamma_{RD} = \frac{\phi P_S}{\sigma_D^2} \max_{n=1, \dots, N_S} |\hat{h}_{1,n}|^2 \sum_{m=1}^{N_D} |h_{2,m}|^2. \tag{18}$$

Due to the impaired detection at R, incorrectly decoded signals might be forwarded to D. Hence, for any modulation strategy, the dual-hop $S \rightarrow R \rightarrow D$ channels can be modeled as an equivalent single hop with output SNR γ_{e2e} . In the medium and high SNR regimes, we can be approximated the output instantaneous SNR of DF protocol, γ_{e2e} , as follows [40, 41]

$$\gamma_{e2e} = \min(\gamma_{SR}, \gamma_{RD}). \tag{19}$$

When γ_{e2e} is in the form of Eq. 19, we can present its CDF as

$$\begin{aligned} F_{\gamma_{e2e}}(x) &= \Pr(\min\{\gamma_{SR}, \gamma_{RD}\} \leq \gamma_{th}) \\ &= 1 - \Pr(\gamma_{SR} > \gamma_{th}, \gamma_{RD} > \gamma_{th}), \end{aligned} \tag{20}$$

where $\gamma_{th} = 2^{2\mathcal{R}/(1-\alpha)} - 1$ denotes the SNR threshold for the relay or the destination node to correctly decode information from the source, with \mathcal{R} be the target information transmission rate.

Thanks to the help of the conditional probability [35], we can recast (20) as

$$F_{\gamma_{e2e}}(x) = 1 - \int_{\zeta}^{\infty} \left[1 - F_{\gamma_{MRC}}\left(\frac{\phi}{x}\right)\right] f_{|\hat{h}_{1,n}|^2}(x) dx, \tag{21}$$

where $\zeta = \frac{\gamma_{th}}{P_S}$.

Substituting (12) and (15)–(21), and applying [32, 8.352.4] lead to the result of Eq. 22, shown at the top of the next page, where $\delta = (1 + (n - 1)(1 - \rho^2))$.

$$F_{\gamma_{e2e}}(x) = 1 - \sum_{n=1}^{N_S} \sum_{k=0}^{N_D-1} \binom{N_S}{n} \frac{n(-1)^{n+1}}{k!\Omega_1\delta} \left(\frac{\phi}{\Omega_2}\right)^k \int_{\zeta}^{\infty} \left(\frac{1}{x}\right)^k \exp\left(-\frac{\phi}{\Omega_2 x} - \frac{nx}{\Omega_1\delta}\right) dx. \tag{22}$$

It is not difficult to see in Eq. 22 that when the lower limit of the integration interval ζ approaching zero, i.e. $\gamma_{th} \ll P_S$, $F_{\gamma_{e2e}}(x)$ is lower bounded by $F_{\gamma_{e2e}}^{Appro}(x)$ of Eq. 23, shown

$$F_{\gamma_{e2e}}^{Appro}(x) = 1 - \sum_{n=1}^{N_S} \sum_{k=0}^{N_D-1} \binom{N_S}{n} \frac{n(-1)^{n+1}}{k!\Omega_1\delta} \left(\frac{\phi x}{\Omega_2}\right)^k {}_2\left(\frac{\phi x \Omega_1 \delta}{n \Omega_2}\right)_{1-k}^{\frac{1-k}{2} \mathcal{K}} \left(2\sqrt{\frac{n \phi x}{\Omega_1 \Omega_2 \delta}}\right). \tag{23}$$

When $\zeta \neq 0$, with the help of the Taylor series for exponential function, i.e., $\exp(-x) = \sum_{q=0}^{\infty} \frac{(-1)^q}{q!} (x)^q$, Eq. 22 is then recast as Eq. 24, shown at the top on the next

at the top of the next page, where, $\mathcal{K}_{1-v}(x)$ is the modified Bessel function first the kind of order $1 - v$.

page. Consider the integral $J(\zeta)$ in (24), let $x = \zeta u$, this leads to $J(\zeta) = \left(\frac{1}{\zeta}\right)^{k+q-1} \int_1^{\infty} \left(\frac{1}{u}\right)^{k+q} \exp\left(-\frac{n\zeta u}{\lambda_1 \delta}\right) du$. For the case $k + q \geq 1$, $J(\zeta)$ is evaluated by [42, 5.1.4],

resulting in Eq. 25a. Otherwise, when $k + q < 1$, it is calculated by [32, 3.381.8], resulting in Eq. 25b. Finally, we

have the exact CDF of the output SNR as shown in Eqs. 24 and Eq. 25a, 25b.

$$F_{\gamma_{e2e}}^{\text{Exact}}(x) = 1 - \left\{ \sum_{n=1}^{N_S} \sum_{k=0}^{N_D-1} \binom{N_S}{n} \frac{n(-1)^{n+1}}{k! \Omega_1 \delta} \sum_{q=0}^{N_I} \frac{(-1)^q}{q!} \left(\frac{\phi \gamma_{\text{th}}}{\Omega_2} \right)^{k+q} J(\zeta) \right\}, \tag{24}$$

$$J(\zeta) = \int_{\zeta}^{\infty} \left(\frac{1}{x} \right)^{k+q} \exp\left(-\frac{nx}{\lambda_1 \delta}\right) dx.$$

$$J(\zeta) = \begin{cases} \left(\frac{1}{\zeta} \right)^{k+q-1} E_{k+q} \left(\frac{n\zeta}{\Omega_1 \delta} \right), & \text{if } k + q \geq 1 \\ \left(\frac{1}{\zeta} \right)^{k+q-1} \left(\frac{n\zeta}{\Omega_1 \delta} \right)^{-(k+q+1)} \Gamma(k + q + 1, \frac{n\zeta}{\Omega_1 \delta}), & \text{if } k + q < 1 \end{cases} \tag{25a}$$

$$\Gamma(k + q + 1, \frac{n\zeta}{\Omega_1 \delta}), \tag{25b}$$

3.2 Outage probability analysis

The outage probability is defined as the probability that instantaneous SNR falls below a threshold γ_{th} , i.e.,

$$\text{OP} = \int_0^{\gamma_{\text{th}}} f_{\gamma_{e2e}}(\gamma) d\gamma = F_{\gamma_{e2e}}(\gamma_{\text{th}}). \tag{26}$$

Substituting (23) or (24)–(26), we obtain the system’s approximate and exact outage probabilities, which are the CDFs of γ_{e2e} with outage threshold γ_{th} .

Other important performance criterion characteristics of diversity systems operating over fading channels are the error probability and capacity or average capacity, which will be analyzed in the following sections.

3.3 Average symbol error probability

In this section, we evaluate the average symbol error probability (SEP) of DF with imperfect CSI over Rayleigh fading. For linearly modulated signals, such as M-PSK, the conditional SEP under an arbitrary SNR, γ_{e2e} , is described by [43]

$$P_e = aQ\left(\sqrt{2b\gamma_{e2e}}\right). \tag{27}$$

Then the average SEP can be determined as

$$\bar{P}_e = \mathbb{E}\left[aQ\left(\sqrt{2b\gamma_{e2e}}\right)\right] = a \int_0^{\infty} Q\left(\sqrt{2b\gamma_{e2e}}\right) f_{\gamma_{e2e}}(\gamma) d\gamma, \tag{28}$$

where $Q(x) = \left(1/\sqrt{2\pi}\right) \int_x^{\infty} e^{-t^2/2} dt$ is the Gaussian Q-function, a and b are the modulation-specific constants. In this work we only consider binary phase-shift keying (BPSK) modulation, hence $a = 1$ and $b = 1$. In the more

general case of M-PSK, $a = 2$ and $b = \sin^2\left(\frac{\pi}{M}\right)$. Following to Eq. 32 in [43], the average SEP can be evaluated as

$$\bar{P}_e = \frac{a\sqrt{b}}{2\sqrt{\pi}} \int_0^{\infty} \frac{e^{-b\gamma}}{\sqrt{\gamma}} F_{\gamma_{e2e}}(\gamma) d\gamma. \tag{29}$$

Replacing the CDF in Eq. 23 or Eqs. 24–29, we can recast the average SEP expression as follows

$$\bar{P}_e = I_1 - I_2, \tag{30}$$

where

$$I_1 = \frac{a\sqrt{b}}{2\sqrt{\pi}} \int_0^{\infty} \frac{e^{-b\gamma}}{\sqrt{\gamma}} d\gamma = \frac{a}{2}, \tag{31}$$

and I_2 is calculated as in Eq. 33 and is approximated as in Eq. 32.

$$I_2^{\text{Appro}} = \sum_{n=1}^{N_S} \sum_{k=0}^{N_D-1} \binom{N_S}{n} \frac{a\sqrt{bn}(-1)^{n+1}}{k! \Omega_1 \delta} \times \left(\frac{1}{\Omega_2} \right)^k \left(\frac{\Omega_1 \delta}{n\Omega_2} \right)^{\frac{1-k}{2}} \phi^{\frac{k+1}{2}} \Gamma\left(1 + \frac{1}{2}\right) \sqrt{\frac{\Omega_1 \Omega_2 \delta}{4n\phi}} \times \exp\left(\frac{n\phi}{2b\Omega_1 \Omega_2 \delta}\right) b^{-\frac{k+1}{2}} W_{-\frac{k+1}{2}, \frac{1-k}{2}}\left(\frac{n\phi}{b\Omega_1 \Omega_2 \delta}\right). \tag{32}$$

where $W_{\ell, \mu}(z)$ denotes the Whittaker function [32].

$$I_2^{\text{Exact}} = \frac{a\sqrt{b}}{2\sqrt{\pi}} \sum_{n=1}^{N_S} \sum_{k=0}^{N_D-1} \sum_{q=0}^{N_I} \frac{n(-1)^{n+1}(-1)^q}{q!k!} \times \binom{N_S}{n} \frac{1}{\Omega_1 \delta} \left(\frac{\phi}{\Omega_2} \right)^{k+q} \left(\frac{n}{\Omega_1 \delta} \right)^{k+q-1} \times \frac{\alpha^v \Gamma(\mu + v)}{\mu(\alpha + \beta)^{\mu+v}} {}_2F_1\left(1, \mu + v; \mu + 1; \frac{\beta}{\alpha + \beta}\right). \tag{33}$$

where $\mu = k + q + \frac{1}{2}$, $\beta = b$, $v = 1 - k - q$ and $\alpha = \frac{n}{\Omega_1 \delta P_S}$. ${}_2F_1(\alpha, \beta; \gamma; z)$ is the Gauss hypergeometric function, please see [32, 9.10 - 9.13]. Further details for I_2^{Appro} and I_2^{Exact} are given in Appendix A. By substituting I_2^{Exact} and I_2^{Appro} into Eq. 30, we obtain the exact and approximate closed-form expressions of SEP of the overall system.

3.4 Average capacity

Based on the end-to-end CDF, shown in Eq. 23, we can analyze the system average capacity. Actually, it is the average mutual information of the S-R-D channel.

Following to the definition of Claude Shannon, the instantaneous channel capacity of our proposed system is given by

$$C = \frac{1 - \alpha}{2} \log_2(1 + \gamma_{e2e}), \tag{34}$$

where the scaling factor $\frac{1-\alpha}{2}$ is accounted for the fact that communication between S and D is carried out in two phases, with $(1 - \alpha)$ is the remaining time for data reception and transmission at R.

From Eq. 34, the average capacity of the system is hence, calculated as

$$\begin{aligned} \bar{C} &= \mathbb{E} \left\{ \frac{1 - \alpha}{2} \log_2(1 + \gamma_{e2e}) \right\} \\ &= \frac{1 - \alpha}{2} \int_0^\infty \log_2(1 + x) f_{\gamma_{e2e}}(x) dx. \end{aligned} \tag{35}$$

Unfortunately, it is impossible to derive the closed-form expression in Eq. 35, and we will resort to some approximations for evaluations. Using the Jensen inequality [44, eq. 4.5], \bar{C} is upper bounded by

$$\bar{C} \leq \frac{(1 - \alpha)}{2} \log_2(1 + \mathbb{E}\{\gamma_{e2e}\}), \tag{36}$$

where $\mathbb{E}(x)$ is the expectation operator. Following to [35, (5-44)], we have $\mathbb{E}\{\gamma_{e2e}\} = \int_0^\infty [1 - F_{\gamma_{e2e}}(x)] dx$.

After some algebraic manipulations, it results in the end-to-end average SNR, $\mathbb{E}\{\gamma_{e2e}\}$, then substituting this into Eq. 36, we get the upper bound of the average capacity as in Eq. 37, shown at the top of the next page.

In the other case, when using the exact CDF as in Eq. 24, then, the upper bound of the average capacity could be evaluated as in Eq. 38, shown at the top of the next page. Please refer to the Appendix B for more details.

$$\begin{aligned} \bar{C} &\leq \frac{1 - \alpha}{2} \log_2 \left(1 + \sum_{n=1}^{N_S} \sum_{k=0}^{N_D-1} \frac{(-1)^{n+1} 2n \Omega_2^k}{k! \delta} \binom{N_S}{n} \left(\frac{\Omega_2 \delta}{n} \right)^{\frac{1-k}{2}} \right. \\ &\quad \left. \times 2^{k+2} \left(\frac{1 - \alpha}{2\alpha\eta P_S} \right)^{\frac{k+1}{2}} \left(\frac{8n\Omega_2(1 - \alpha)}{\delta 2\alpha\eta P_S} \right)^{-\frac{3-k}{2}} \Gamma\left(\frac{1}{2}\right) \Gamma\left(1 + \frac{1}{2}\right) \right). \end{aligned} \tag{37}$$

$$\begin{aligned} \bar{C} &\leq \frac{1 - \alpha}{2} \log_2 \left(1 + \sum_{n=1}^{N_S} \sum_{k=0}^{N_D-1} \binom{N_S}{n} \frac{n(-1)^{n-1}}{\lambda_1 \delta k!} \left(\frac{n}{\lambda_1 \delta} \right)^{-2} \varphi(q) \right), \\ \text{where } \varphi(q) &= \sum_{q=0}^{N_t} \frac{(-1)^q}{q! (k + q + 1)} \left(\frac{1}{P_S} \right)^{-k-q-1} \left(\frac{\phi}{\lambda_2} \right)^{k+q}. \end{aligned} \tag{38}$$

4 Simulation results

In this section, we verify our analysis by comparing the theoretical results with the Monte-Carlo simulation counterparts. We also study the effect of the number of antennas at source and destination nodes on the outage probability and symbol error probability. Unless otherwise notified, system model parameters are set up as follows. Energy harvesting duration is $\alpha = 0.3$. RF power conversion efficiency is almost close to perfect, $\eta = 0.95$. Channel correlation coefficient is $\rho = 0.95$. Distance from the source node to the destination node is normalized to

unity. The relay node is located right between the source and destination nodes. Target rate is $\mathcal{R} = 1$ [bpcu] with BPSK signaling.

Figure 3 shows the system outage probabilities versus SNR calculated by both (Monte-Carlo) numerical and analytical methods. The analytical results are taken from both approximate (23) and exact (24) expressions. Three different antenna configurations are in consideration, namely, $[N_S N_D] = [1 1], [2 1],$ and $[2 2]$. It can be observed that the derived analytical results reasonably match with the simulation ones, confirming the correctness of the derivations. Specifically, the exact calculations

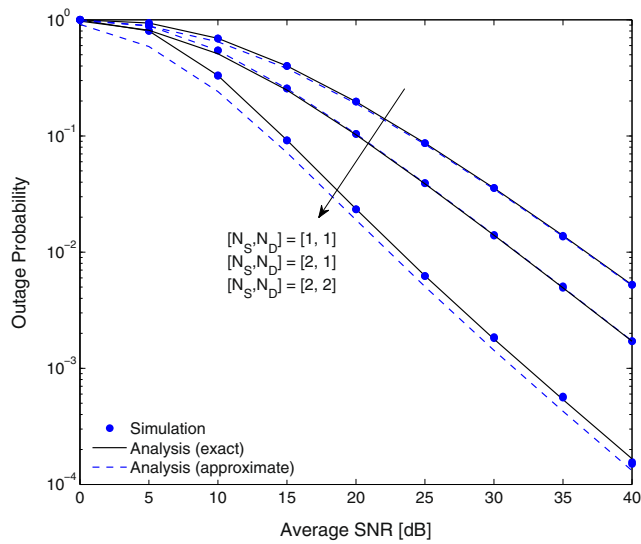


Fig. 3 Outage probability versus average SNRs with $\alpha = 0.3$, $\rho = 0.95$, and different transmit/receive antenna configurations

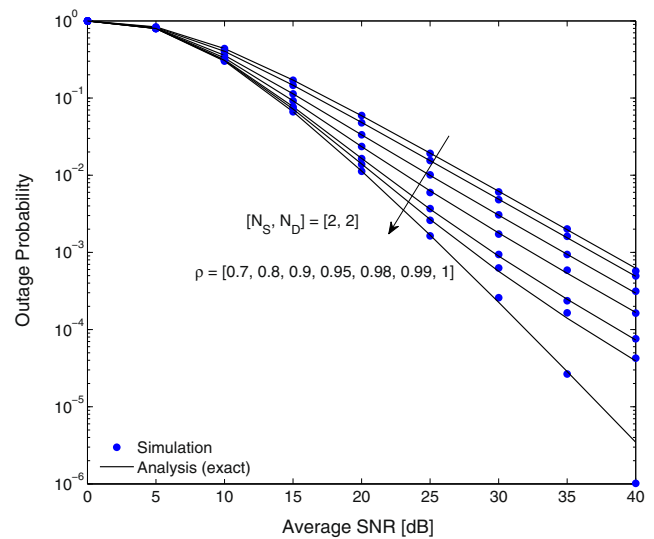


Fig. 4 Outage probability versus average SNR with $N_S = 2$, $N_D = 2$, $\alpha = 0.3$ and different correlation coefficients ρ

of Eq. 24 perfectly agree with the numerical results. Moreover, the analytical approximations by Eq. 23 get better accuracies when increasing SNR. Therefore, it can be used for precisely estimating the system outage probability with a relatively low complexity. With relatively high channel correlation coefficient $\rho = 0.95$, it is observed that increasing number antennas leads to system performance improvement. Further, although using 0.3 period for energy harvesting, at high SNR, the system diversity order still approximates to 2 in scenario $[N_S \ N_D] = [2 \ 2]$.

The effects of channel correlation ρ to the system outage probability is illustrated in Fig. 4. In this case, we use the antenna configuration of $[N_S \ N_D] = [2 \ 2]$ and the exact analysis of Eq. 24 for reference. The curves show that increasing ρ , i.e. decreasing feedback delay, results in an improvement in the outage probability performance. However, the improvement is only significant for ρ closely approaching to 1. Hence, the channel correlation, or equivalently the feedback delay, has strong effect to the system performance. The regularity of R-to-S feedback should be frequent enough for the expectation of great system performance improvement. Otherwise, the use of multi antennas at D has little meaning.

In Fig. 5, we investigate the effect of CSI imperfection on the TAS scheme in terms of SEP, considering to the curves with $[N_S, N_D] = [2, 1]$. As also being observed for OP from previous figure, for $0.8 \leq \rho \leq 0.9$, there is a little improvement in SEP, while for ρ approaching to 1, the SEP performance dramatically get better. In this figure, we also compare the proposed system to the counterpart without EH [30]. For equality in comparison, the CSI is assume to be perfect, $\rho = 1$. Spending 0.33 period of time for harvesting energy, but the SNR loss in our system is not significant

compared to the counterpart without EH to guarantee the same SEP (maximally, about 1.7 dB at the SEP = 5.10^{-6}). This certifies the applicability of our proposal in practice, considering to the energy saving and simplicity of the relay node. Moreover, the well match of analytical and numerical SEP results again confirm the correctness of the derivations.

We inspect the effects of S's antenna number to the system SEP in Fig. 6. When increasing N_S from 1 to 2, the system gains large improvement in SEP. While $N_S = 3$, the SEP gain is actually insignificant. Thus, the increase in the number of antenna of S does not result in diversity order gain but provide the diversity gain for the operation of TAS scheme. Therefore, it is not necessary to deploy

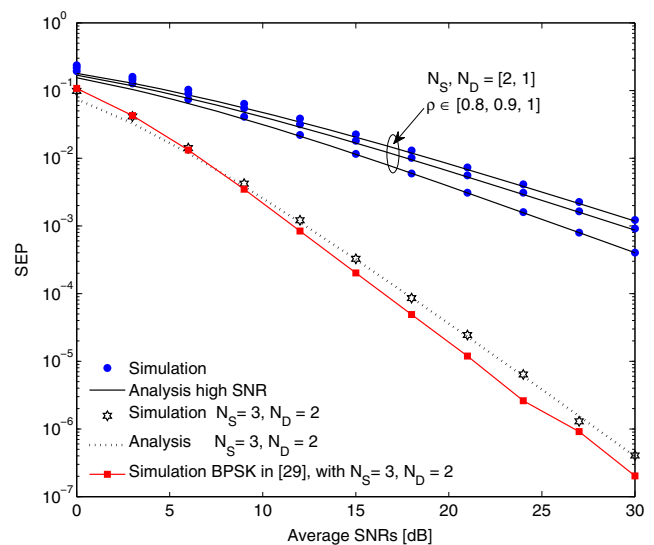


Fig. 5 Symbol error probability versus average SNR with different antenna configurations and correlation coefficients ρ

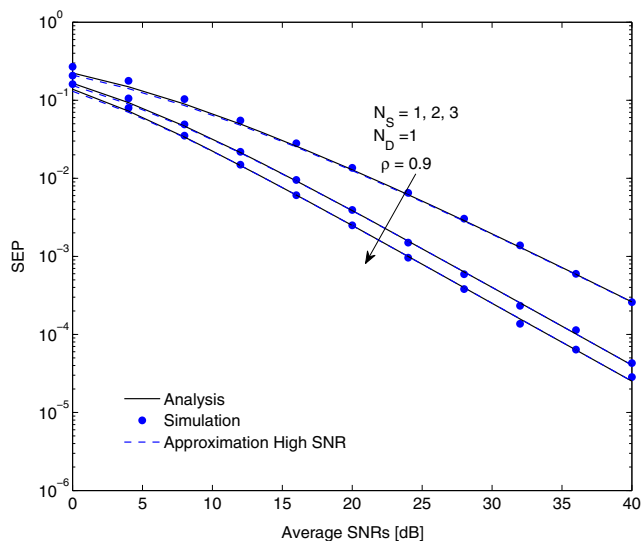


Fig. 6 Symbol error probability versus average SNR with $\rho = 0.9$ and different number of antennas

so many antennas at the source node because the reward is not adequate. However, for a higher requirement of SEP performance, the increasing of antenna number at S is also an option.

Diversity order is verified in Fig. 7, where different antenna configurations are used for simulating SEP. Although using $\alpha = 0.33$ period of time for harvesting energy, the diversity order of the proposed system is guaranteed by antenna number at D as can be seen from these curves.

Figure 8 plots the system ergodic capacities versus SNR. Analytic results are upper bounded using Jensen inequality (36). This is a trade-off between complexity and accuracy

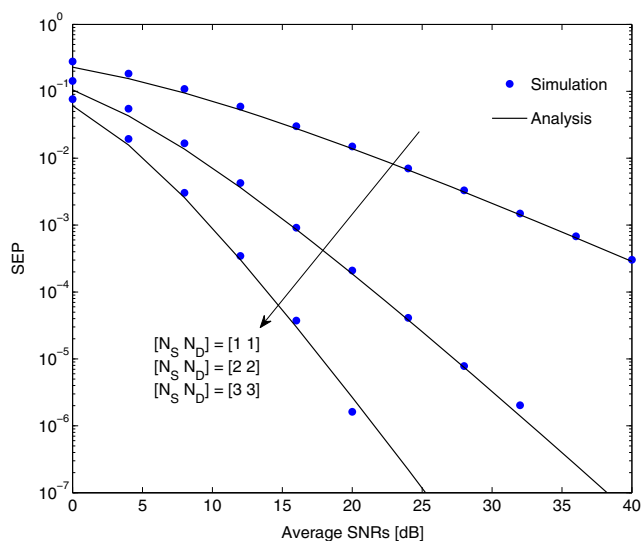


Fig. 7 Symbol error probability versus average SNR with $\rho = 1$, $\eta = 0.85$ and different number of antennas

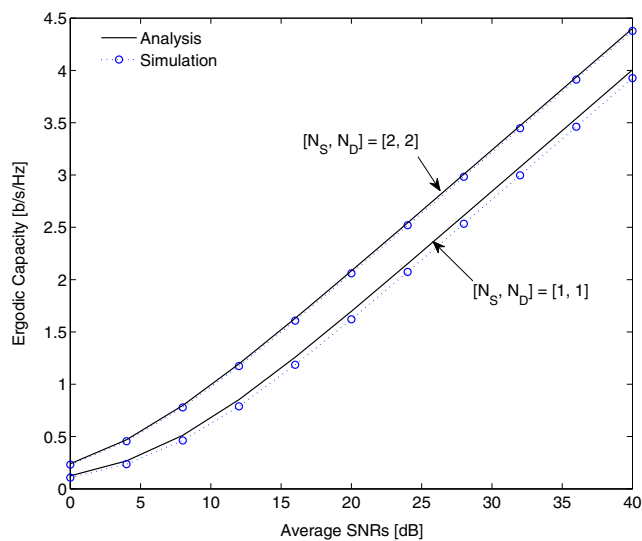


Fig. 8 Exact and approximate ergodic capacities versus average SNR with $\rho = 1$ and different number of antennas

for the difficulties in calculating the exact ergodic capacity. Results in the figure show that this trade-off is acceptable. Further, we can see that different numbers of antennas, i.e. $[N_S, N_D] = [2, 2]$ and $[N_S, N_D] = [2, 1]$, result in different accuracies, i.e. the larger number of antenna, the better approximation. This is because number of terms in summation in Eq. 37 increases by number of antennas. As seen in Fig. 8 the numerical results are well close to the analytical (upper bounded) results, hence, it is reasonable to use Jensen approximation for determining the ergodic capacity.

In Fig. 9, we investigate the effects of channel correlation to the system average capacity. It is observed that ρ strongly

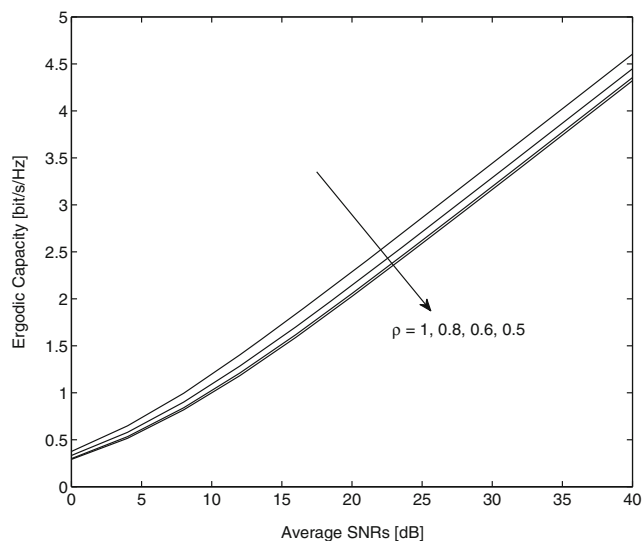


Fig. 9 Ergodic capacity versus average SNR with $N_S = 2$, $N_D = 2$ and different correlation coefficients

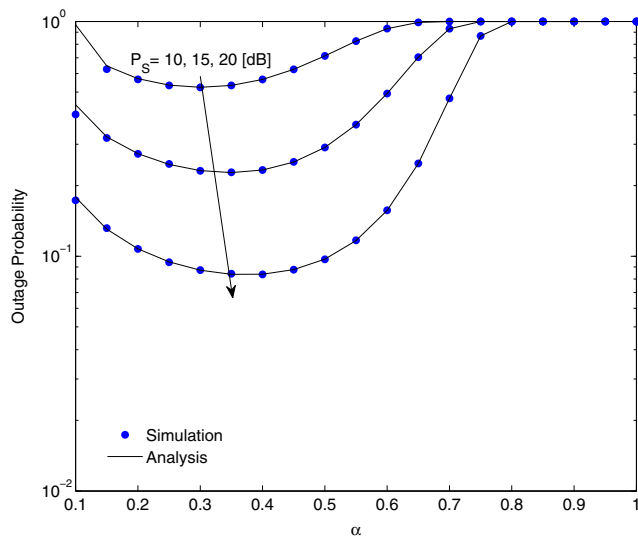


Fig. 10 Outage probability of the MIMO-SWIPT relay network versus α with $\rho = 1$, $N_S = 1$, $N_D = 1$ and different transmit power levels

affects the system average capacity. Specifically, $\rho \leq 0.8$ significantly reduces the system capacity.

Figure 10 demonstrates the impact of the fraction harvesting energy duration $0 < \alpha < 1$ on the OP. Actually, the optimal α is a complicated function of channel and system parameters. Smaller α results in smaller energy for R but larger α also yields smaller transmit power (at S) for communication. Therefore, as the energy harvesting ratio α increases from 0 to 1, the system OP reduces to an optimal value then increases again. The optimal α corresponding to

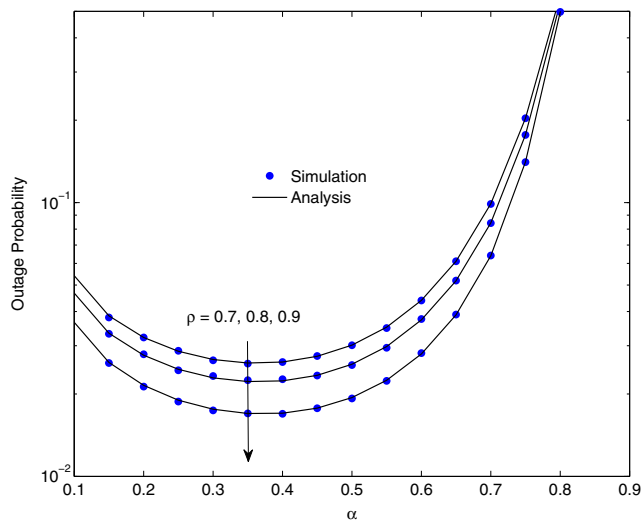


Fig. 11 Outage probability versus energy harvesting ratio α with different channel correlation coefficients ρ

the smallest OP is then determined by this plot. Roughly, this value is $\alpha = 0.33$, insensitive to the transmit power P_S .

We again investigate the sensitivity of the OP by the channel correlation ρ in Fig. 11. Obviously, larger ρ gives better OP. As be seen from these curves, $\alpha = 0.33$ results in optimal OP, insensitive to the channel correlations.

5 Conclusions

In this paper, we investigate the performance of MIMO SWIPT relay network under imperfect CSI. We derive the exact and approximate closed-form expressions for outage probability. Using Jensen inequality, we calculate the upper bound for ergodic capacity. Further, the exact and approximate SEPs are also figured out. Our results can be used to quantify the effect of time delay or channel estimation error on the TAS scheme at the source node and the relay node using DF scheme. Based on these results, optimal energy harvesting duration is found out. For this value, the proposed system acquires almost the same performance compared to the counterpart without using energy harvesting.

Appendix A

Aiming at the closed-form formulations for I_2^{Exact} and I_2^{Appro} , we start by determining the corresponding constituent integral as follows: Substituting (23)–(29) and carrying out some manipulations, we have

$$I_2^{\text{Appro}} = \frac{a\sqrt{b}}{2\sqrt{\pi}} \sum_{n=1}^{N_S} \sum_{k=0}^{N_D-1} \binom{N_S}{n} \frac{n(-1)^{n+1}}{\lambda_1 \delta} 2 \left(\frac{\phi \lambda_1 \delta}{n \lambda_2} \right)^{\frac{1-k}{2}} \times \int_0^\infty \frac{e^{-bx}}{\sqrt{x}} x^{\frac{1-k}{2}} \left(\frac{\phi x}{\lambda_2} \right)^k \mathcal{K}_{1-k} \left(2\sqrt{\frac{n\phi x}{\lambda_1 \lambda_2 \delta}} \right) dx. \tag{39}$$

With the help of [32, 6.643.3], I_2^{Appro} is then obtained as in Eq. 32.

Similarly, for the case of I_2^{Exact} , substituting the exact CDF in Eqs. 24–29, it hence is recast as

$$I_2^{\text{Exact}} = \frac{a\sqrt{b}}{2\sqrt{\pi}} \int_0^\infty \frac{e^{-bx}}{\sqrt{x}} \sum_{n=1}^{N_S} \sum_{k=0}^{N_D-1} \sum_{q=0}^{N_I} \frac{n(-1)^{n+1}}{q!k!} \left(\frac{\phi}{\Omega_2} \right)^{k+q} \times \binom{N_S}{n} \frac{P_S^{k+q-1} (-1)^q}{\Omega_1 \delta} x E_{k+q} \left(\frac{nx}{\Omega_1 \delta P_S} \right) dx. \tag{40}$$

With the help of [42, 5.1.45], and using $E_n(z) = z^{n-1} \Gamma(1-n, z)$, I_2^{Exact} can then be recast as

$$I_2^{\text{Exact}} = \frac{a\sqrt{b}}{2\sqrt{\pi}} \sum_{n=1}^{N_S} \sum_{k=0}^{N_D-1} \sum_{q=0}^{N_i} \frac{n(-1)^{n+1}(-1)^q}{q!k!} \times \binom{N_S}{n} \frac{1}{\Omega_1\delta} \left(\frac{\phi}{\Omega_2}\right)^{k+q} \left(\frac{n}{\Omega_1\delta}\right)^{k+q-1} \times \underbrace{\int_0^\infty e^{-bx} x^{k+q+\frac{1}{2}-1} \Gamma\left(1-k-q, \frac{nx}{\Omega_1\delta P_S}\right) dx}_{\mathcal{I}(x)}. \tag{41}$$

For calculating $\mathcal{I}(x)$, [32, 6.455.1] is applied, and after some manipulations, we have

$$\mathcal{I}(x) = \frac{\alpha^v \Gamma(\mu+v)}{\mu(\alpha+\beta)^{\mu+v}} {}_2F_1\left(1, \mu+v; \mu+1; \frac{\beta}{\alpha+\beta}\right). \tag{42}$$

Using the [32, 3.361.2], we then obtain the closed-form formulation of I_2^{Exact} .

Appendix B

Starting from statistical expectation formulation $\mathbb{E}\{\gamma_{e2e}\} = \int_0^\infty [1 - F_{\gamma_{e2e}}(x)] dx$ with the CDF of (23), after some manipulations, we can rewrite $\mathbb{E}\{\gamma_{e2e}\}$ as

$$\mathbb{E}\{\gamma_{e2e}\} = \sum_{n=1}^{N_S} \sum_{k=0}^{N_D-1} \binom{N_S}{n} \frac{1}{k!} \frac{n(-1)^{n+1}}{\lambda_1\delta} \left(\frac{\phi}{\lambda_2}\right)^k \times 2 \left(\frac{\phi\lambda_1\delta}{n\lambda_2}\right)^{\frac{1-k}{2}} \int_0^\infty x^{\frac{k+1}{2}} \mathcal{K}_{1-k}\left(\sqrt{\frac{4n\phi x}{\lambda_1\lambda_2\delta}}\right) dx. \tag{43}$$

Let $\sqrt{x} = u$ and using [32, 6.561.16], we then have $\mathbb{E}\{\gamma_{e2e}\}$ expressed as

$$\mathbb{E}\{\gamma_{e2e}\} = \sum_{n=1}^{N_S} \sum_{k=0}^{N_D-1} \binom{N_S}{n} 2 \left(\frac{\lambda_2\delta}{n}\right)^{\frac{1-k}{2}} 2^{k+2} \left(\frac{1-\alpha}{2\alpha\eta P_S}\right)^{\frac{k+1}{2}} \times \left(\frac{8n\lambda_2(1-\alpha)}{\delta 2\alpha\eta P_S}\right)^{-\frac{3-k}{2}} \Gamma\left(\frac{1}{2}\right) \Gamma\left(1+\frac{1}{2}\right). \tag{44}$$

Substituting (44)–(36), we then have the average capacity formulation of Eq. 37.

Similarly, the average end-to-end SNR is given by

$$\mathbb{E}\{\gamma_{e2e}\} = \sum_{n=1}^{N_S} \sum_{k=0}^{N_D-1} \frac{1}{k!} \frac{n(-1)^{n+1}}{\lambda_1\delta} \times \sum_{q=0}^{N_i} \frac{(-1)^q P_S^{k+q-1} \left(\frac{\phi}{\lambda_2}\right)^{k+q}}{q!} \times \int_0^\infty x E_{k+q}\left(\frac{nx}{P_S\lambda_1\delta}\right) dx. \tag{45}$$

With the help of [42, 5.1.45], we can rewrite (45) as

$$\mathbb{E}\{\gamma_{e2e}\} = \sum_{n=1}^{N_S} \sum_{k=0}^{N_D-1} \sum_{q=0}^{N_i} \frac{(-1)^q n(-1)^{n-1}}{\lambda_1\delta k! q!} \times \binom{N_S}{n} \left(\frac{\phi}{\lambda_2}\right)^{k+q} \left(\frac{n}{\lambda_1\delta}\right)^{k+q-1} \times \int_0^\infty x^{k+q} \Gamma\left(1-(k+q), \frac{nx}{P_S\lambda_1\delta}\right) dx. \tag{46}$$

Thank to the help of [42, 6.5.37], and after some modifications, we have

$$\mathbb{E}\{\gamma_{e2e}\} = \sum_{n=1}^{N_S} \sum_{k=0}^{N_D-1} \binom{N_S}{n} \frac{n(-1)^{n-1}}{\lambda_1\delta k!} \left(\frac{n}{\lambda_1\delta}\right)^{-2} \times \sum_{q=0}^{N_i} \frac{(-1)^q}{q!(k+q+1)} \left(\frac{1}{P_S}\right)^{-k-q-1} \left(\frac{\phi}{\lambda_2}\right)^{k+q}. \tag{47}$$

Replacing (47)–(36), we then obtain the average capacity as in Eq. 38.

References

1. David K, Berndt H (2018) 6G vision and requirements: is there any need for beyond 5G. *IEEE Veh Technol Mag* (13):72–80
2. Nguyen LD (2018) Resource allocation for energy efficiency in 5G wireless networks. *EAI Endorsed Trans Ind Netw Intell Syst* 5:14
3. Varshney LR (2008) Transporting information and energy simultaneously. In: *Proceedings of 2008 IEEE international symposium on information theory*. IEEE, pp 1612–1616
4. Lu X, Wang P, Niyato D, Kim DI, Han Z (2015) Wireless networks with RF energy harvesting: a contemporary survey. *IEEE Commun Surv Tutor* 17(2):757–789
5. Zhang R, Ho CK (2013) MIMO Broadcasting for simultaneous wireless information and power transfer. *IEEE Trans Commun* 12(5):1989–2001
6. Zhou X, Zhang R, Ho CK (2013) Wireless information and power transfer: architecture design and rate-energy tradeoff. *IEEE Trans Commun* 61(11):4754–4767
7. Ding Z, Perlaza SM, Esnaola I, Poor HV (2014) Power allocation strategies in energy harvesting wireless cooperative networks. *IEEE Trans Wirel Commun* 13(2):846–860

8. Nasir AA, Zhou X, Durrani S, Kennedy RA (2013) Relaying protocols for wireless energy harvesting and information processing. *IEEE Trans Wirel Commun* 12(7):3622–3636
9. Do NT, da Costa DB, Duong TQ, Bao VNQ, An B (2017) Exploiting direct links in multiuser multirelay SWIPT cooperative networks with opportunistic scheduling. *IEEE Trans Wirel Commun* 16(8):5410–5427
10. Dong Y, Hossain MJ, Cheng J (2016) Performance of wireless powered amplify and forward relaying over nakagami- m fading channels with nonlinear energy harvester. *IEEE Commun Lett* 20(4):672–675
11. Do TN, da Costa DB, Duong TQ, An B (2018) Improving the performance of cell-edge users in MISO-NOMA systems using TAS and SWIPT-based cooperative transmissions. *IEEE Trans Green Commun Netw* 2(1):49–62
12. Do NT, Da Costa DB, Duong TQ, An B (2017) A BNB user selection scheme for NOMA-based cooperative relaying systems with SWIPT. *IEEE Commun Lett* 21(3):664–667
13. Hoang TM, Van Son V, Dinh NC, Hiep PT (2018) Optimizing duration of energy harvesting for downlink NOMA full-duplex over Nakagami- m fading channel. *AEU-Int J Electron Commun* 95:199–206
14. Hoang TM, Tan NT, Hoang NH, Hiep PT Performance analysis of decode-and-forward partial relay selection in NOMA systems with RF energy harvesting, *Wireless Networks*, pp 1–11. <https://doi.org/10.1007/s11276-018-1746-8>
15. Radaydeh RM (2009) Impact of delayed arbitrary transmit antenna selection on the performance of rectangular QAM with receive MRC in fading channels. *IEEE Commun Lett* 6:13
16. Suraweera HA, Soysa M, Tellambura C, Garg HK (2010) Performance analysis of partial relay selection with feedback delay. *IEEE Signal Process Lett* 17(6):531–534
17. Michalopoulos DS, Chatzidiamentis ND, Schober R, Karagiannidis GK (2011) Relay selection with outdated channel estimates in Nakagami- m fading. In: *Proceedings of 2011 IEEE international conference on communications (ICC)*. IEEE, pp 1–6
18. Ferdinand NS, da Costa DB, Latva-aho M (2013) Effects of outdated CSI on the secrecy performance of MISO wiretap channels with transmit antenna selection. *IEEE Commun Lett* 17(5):864–867
19. Amarasuriya G, Larsson EG, Poor HV (2016) Wireless information and power transfer in multiway massive MIMO relay networks. *IEEE Trans Wirel Commun* 15(6):3837–3855
20. Zhao L, Wang X, Zheng K (2016) Downlink hybrid information and energy transfer with massive MIMO. *IEEE Trans Wirel Commun* 15(2):1309–1322
21. Shi Q, Xu W, Wu J, Song E, Wang Y (2015) Secure beamforming for MIMO broadcasting with wireless information and power transfer. *IEEE Trans Wirel Commun* 14(5):2841–2853
22. Zhang Q, Li Q, Qin J (2016) Beamforming design for OSTBC-based AF-MIMO two-way relay networks with simultaneous wireless information and power transfer. *IEEE Trans Veh Commun* 65(9):7285–7296
23. Bao VNQ, Duong TQ, Tellambura C (2013) On the performance of cognitive underlay multihop networks with imperfect channel state information. *IEEE Trans Wirel Commun* 61(12):4864–4873
24. Fan L, Lei X, Yang N, Duong TQ, Karagiannidis GK (2017) Secrecy cooperative networks with outdated relay selection over correlated fading channels. *IEEE Trans Veh Commun* 66(8):7599–7603
25. Huang Y, Al-Qahtani FS, Duong TQ, Wang J (2015) Secure transmission in MIMO wiretap channels using general-order transmit antenna selection with outdated CSI. *IEEE Trans Wirel Commun* 63(8):2959–2971
26. Lee K, Hong J-P (2016) Energy-efficient resource allocation for simultaneous information and energy transfer with imperfect channel estimation. *IEEE Trans Veh Commun* 65(4):2775–2780
27. Benkhelifa F, Salem AS, Alouini M-S (2016) Rate maximization in MIMO decode-and-forward communications with an EH relay and possibly imperfect CSI. *IEEE Trans Wirel Commun* 64(11):4534–4549
28. Prasad B, Roy SD, Kundu S (2015) Secondary throughput in underlay cognitive radio network with imperfect CSI and energy harvesting relay. In: *Proceedings of 2015 IEEE international conference on advanced networks and telecommunications systems (ANTS)*. IEEE, pp 1–6
29. Zhang J, Pan G (2016) Outage analysis of wireless-powered relaying MIMO systems with non-linear energy harvesters and imperfect CSI. *IEEE Access* 4:7046–7053
30. Yilmaz A, Kucur O (2012) Performance of transmit antenna selection and maximal-ratio combining in dual hop amplify-and-forward relay network over Nakagami- m fading channels. *Wirel Pers Commun* 3(67):485–503
31. Mohammadi M, Chalise BK, Suraweera HA, Zhong C, Zheng G, Krikidis I (2016) Throughput analysis and optimization of wireless-powered multiple antenna full-duplex relay systems. *IEEE Trans Commun* 64(4):1769–1785
32. Gradshteyn IS, Ryzhik IM (2014) *Table of integrals, series, and products*. Academic Press, Cambridge
33. Rajesh R, Sharma V, Viswanath P (2014) Capacity of gaussian channels with energy harvesting and processing cost. *IEEE Trans Inf Theory* 60(5):2563–2575
34. Suraweera HA, Smith PJ, Shafi M (2010) Capacity limits and performance analysis of cognitive radio with imperfect channel knowledge. *IEEE Trans Veh Commun* 59(4):1811–1822
35. Papoulis A, Pillai SU (2002) *Probability, random variables, and stochastic processes*. Tata McGraw-Hill Education, New York
36. Ahn KS, Heath JRW (2009) Performance analysis of maximum ratio combining with imperfect channel estimation in the presence of cochannel interferences. *IEEE Trans Wirel Commun* 8(3):1080–1085
37. Simon MK, Alouini M-S (2002) *Digital communication over generalized fading channels: a unified approach to performance analysis*. Wiley, New York
38. Van Khuong H, Kong H-Y (2006) General expression for eps of a sum of independent exponential random variables. *IEEE Commun Lett* 10(3):159–161
39. Tang J, Zhang X (2006) Transmit selection diversity with maximal-ratio combining for multicarrier DS-CDMA wireless networks over Nakagami- m fading channels. *IEEE J Sel Areas Commun* 24(1):104–112
40. Bao VNQ, Kong HY (2010) Performance analysis of decode-and-forward relaying with partial relay selection for multihop transmission over Rayleigh fading channels. *J Commun Netw* 12(5):433–441
41. Laneman JN, Tse DN, Wornell GW (2004) Cooperative diversity in wireless networks: efficient protocols and outage behavior. *IEEE Trans Inf Theory* 50(12):3062–3080
42. Abramowitz M, Stegun IA (1965) *Handbook of mathematical functions: with formulas, graphs, and mathematical tables*. Dover Publications, New York
43. Chen Y, Tellambura C (2004) Distribution functions of selection combiner output in equally correlated Rayleigh, Rician, and Nakagami- m fading channels. *IEEE Trans Wirel Commun* 52(11):1948–1956
44. Goldsmith A (2005) *Wireless communications*. Cambridge University Press, Cambridge